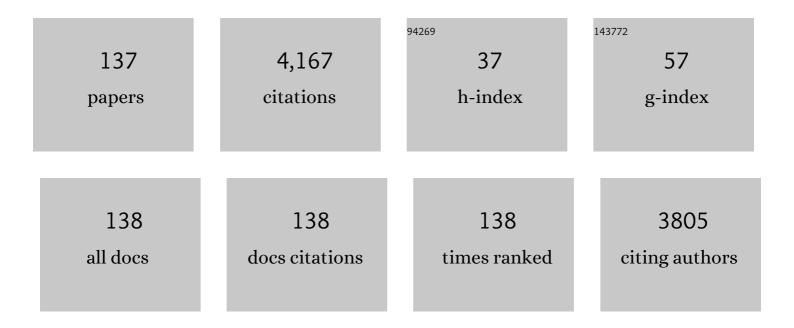
List of Publications by Year in descending order

Source: https://exaly.com/author-pdf/1230567/publications.pdf Version: 2024-02-01



#	Article	IF	CITATIONS
1	Prediction and experimental evaluation of the threshold velocity in water droplet erosion. Materials and Design, 2022, 213, 110312.	3.3	16
2	Stability of the microstructure and elevated-temperature mechanical properties of additively manufactured Inconel 718 superalloy subjected to long-term in-service thermal cycling. Materials Science & Engineering A: Structural Materials: Properties, Microstructure and Processing, 2022, 838, 142790.	2.6	6
3	Experimental and CFD simulation of interactions between water droplets with different surface features to understand water droplet erosion. Transactions of the Canadian Society for Mechanical Engineering, 2022, 46, 573-586.	0.3	2
4	On the role of strain hardening and mechanical properties in water droplet erosion of metals. Tribology International, 2022, 173, 107649.	3.0	5
5	Optimization of the Post-Process Heat Treatment of Inconel 718 Superalloy Fabricated by Laser Powder Bed Fusion Process. Metals, 2021, 11, 144.	1.0	12
6	Optimization of the Electrospun Niobium–Tungsten Oxide Nanofibers Diameter Using Response Surface Methodology. Nanomaterials, 2021, 11, 1644.	1.9	4
7	Water droplet impingement erosion performance of WC-based coating sprayed by HVAF and HVOF. Wear, 2021, 484-485, 203904.	1.5	14
8	Effect of homogenization and solution treatments time on the elevated-temperature mechanical behavior of Inconel 718 fabricated by laser powder bed fusion. Scientific Reports, 2021, 11, 2020.	1.6	46
9	Water Droplet Erosion of Wind Turbine Blades: Mechanics, Testing, Modeling and Future Perspectives. Materials, 2020, 13, 157.	1.3	50
10	Influence of Homogenization and Solution Treatments Time on the Microstructure and Hardness of Inconel 718 Fabricated by Laser Powder Bed Fusion Process. Materials, 2020, 13, 2574.	1.3	37
11	Power Ultrasonic Additive Manufacturing: Process Parameters, Microstructure, and Mechanical Properties. Advances in Materials Science and Engineering, 2020, 2020, 1-17.	1.0	14
12	Investigation on metallic glass formation in Mg-Zn-Sr ternary system combined with the CALPHAD method. Materials Letters, 2019, 256, 126628.	1.3	8
13	Hot compression behavior and microstructure of selectively laser-melted IN718 alloy. International Journal of Advanced Manufacturing Technology, 2018, 96, 371.	1.5	21
14	Magnetic force microscopic study of Ce2(Fe, Co)14B, and its modifications by Ni and Cu. Journal of Magnetism and Magnetic Materials, 2018, 460, 95-103.	1.0	9
15	Intrinsic Magnetic Properties of Ce2Fe14B Modified by Al, Ni, or Si. Applied Sciences (Switzerland), 2018, 8, 205.	1.3	13
16	Phase equilibria and magnetic phases in the Fe-rich regions of the Ce-Fe-{Ni, Si, Al}-B quaternary systems. Journal of Alloys and Compounds, 2018, 763, 289-295.	2.8	4
17	Microstructural and Microhardness Evolution from Homogenization and Hot Isostatic Pressing on Selective Laser Melted Inconel 718: Structure, Texture, and Phases. Journal of Manufacturing and Materials Processing, 2018, 2, 30.	1.0	33
18	Intrinsic magnetic properties of Ce2(Fe, Co)14B and its modifications by Ni and Cu. Journal of Alloys and Compounds, 2018, 763, 916-925.	2.8	3

#	Article	IF	CITATIONS
19	Microstructure, In Vitro Corrosion Behavior and Cytotoxicity of Biodegradable Mg-Ca-Zn and Mg-Ca-Zn-Bi Alloys. Journal of Materials Engineering and Performance, 2017, 26, 653-666.	1.2	28
20	Thermal Characteristics, Mechanical Properties, In Vitro Degradation and Cytotoxicity of Novel Biodegradable Zn–Al–Mg and Zn–Al–Mg–xBi Alloys. Acta Metallurgica Sinica (English Letters), 2017, 30, 201-211.	1.5	39
21	Characterisation and thermodynamic calculations of biodegradable Mg–2.2Zn–3.7Ce and Mg–Ca–2.2Zn–3.7Ce alloys. Materials Science and Technology, 2017, 33, 1333-1345.	0.8	7
22	Phase Equilibria and Magnetic Phases in the Ce-Fe-Co-B System. Materials, 2017, 10, 16.	1.3	14
23	Binary Phase Diagrams and Thermodynamic Properties of Silicon and Essential Doping Elements (Al, As,) Tj ETQq1	1,0.7843	14 rgBT /C
24	Structure, Texture and Phases in 3D Printed IN718 Alloy Subjected to Homogenization and HIP Treatments. Metals, 2017, 7, 196.	1.0	179
25	Water Droplet Erosion Performance of Laser Shock Peened Ti-6Al-4V. Metals, 2016, 6, 262.	1.0	17
26	Energy based approach for understanding water droplet erosion. Materials and Design, 2016, 104, 76-86.	3.3	22
27	Experimental investigation of the Mg Zn Zr ternary system at 450°C. Journal of Alloys and Compounds, 2016, 680, 212-225.	2.8	7
28	Novel bi-layered nanostructured SiO2/Ag-FHAp coating on biodegradable magnesium alloy for biomedical applications. Ceramics International, 2016, 42, 11941-11950.	2.3	42
29	Effect of ultrasonic nanocrystalline surface modification on the water droplet erosion performance of Ti 6Al 4V. Surface and Coatings Technology, 2016, 307, 157-170.	2.2	34
30	Preparation and Performance of Plasma/Polymer Composite Coatings on Magnesium Alloy. Journal of Materials Engineering and Performance, 2016, 25, 3948-3959.	1.2	12
31	Thermodynamic analysis of dehydrogenation path of Mg–Al–Li–Na alloys. Calphad: Computer Coupling of Phase Diagrams and Thermochemistry, 2016, 54, 54-66.	0.7	3
32	HVOF and HVAF Coatings of Agglomerated Tungsten Carbide-Cobalt Powders for Water Droplet Erosion Application. Journal of Thermal Spray Technology, 2016, 25, 1711-1723.	1.6	12
33	Understanding the hydrogen storage behavior of promising Al–Mg–Na compositions using thermodynamic modeling. Materials for Renewable and Sustainable Energy, 2016, 5, 1.	1.5	3
34	Water droplet erosion behaviour of gas nitrided Ti6Al4V. Surface and Coatings Technology, 2016, 292, 78-89.	2.2	23
35	Fabrication and characterization of hydrophobic microarc oxidation/poly-lactic acid duplex coating on biodegradable Mg–Ca alloy for corrosion protection. Vacuum, 2016, 125, 185-188.	1.6	61
36	Thermodynamic modelling and in-situ neutron diffraction investigation of the (Ce + Mg + Zn) system. Journal of Chemical Thermodynamics, 2016, 93, 242-254.	1.0	6

#	Article	IF	CITATIONS
37	Preparation and characterization of NiCrAlY/nano-YSZ/PCL composite coatings obtained by combination of atmospheric plasma spraying and dip coating on Mg–Ca alloy. Journal of Alloys and Compounds, 2016, 658, 440-452.	2.8	65
38	Water Impingement Erosion of Deep-Rolled Ti64. Metals, 2015, 5, 1462-1486.	1.0	27
39	Experimental Investigation of the Mg-Nd-Zn Isothermal Section at 300 ŰC. Metals, 2015, 5, 84-101.	1.0	15
40	Experimental Study of the Mg-Ni-Y System at 673 K Using Diffusion Couples and Key Alloys. Metals, 2015, 5, 1746-1769.	1.0	17
41	Corrosion and mechanical performance of double-layered nano-Al/PCL coating on Mg–Ca–Bi alloy. Vacuum, 2015, 119, 95-98.	1.6	33
42	Thermodynamic modeling of Cu–Ni–Y system coupled with key experiments. Materials Chemistry and Physics, 2015, 153, 32-47.	2.0	7
43	Effect of Electrodeposition Parameters on the Microstructure and Corrosion Behavior of ‎ <scp>DCPD</scp> Coatings on Biodegradable <scp>M</scp> g– <scp>C</scp> a– <scp>Z</scp> n Alloy. International Journal of Applied Ceramic Technology, 2015, 12, 1054-1064.	1.1	17
44	Experimental study of the crystal structure of the Mg15â^'xZnxSr3 ternary solid solution in the Mg–Zn–Sr system at 300°C. Materials and Design, 2015, 86, 305-312.	3.3	21
45	Synthesis and corrosion behavior of a hybrid bioceramic-biopolymer coating on biodegradable Mg alloy for orthopaedic implants. Journal of Alloys and Compounds, 2015, 648, 1067-1071.	2.8	31
46	Experimental study of the phase equilibria in the Mg–Zn–Ag ternary system at 300 °C. Journal of Alloys and Compounds, 2015, 639, 593-601.	2.8	37
47	Experimental determination of the phase equilibria in the Mg–Zn–Sr ternary system. Journal of Materials Science, 2015, 50, 7636-7646.	1.7	22
48	The effect of initial surface roughness on water droplet erosion behaviour. Wear, 2015, 342-343, 198-209.	1.5	70
49	Microstructural, mechanical properties and corrosion behavior of plasma sprayed NiCrAlY/nano-YSZ duplex coating on Mg–1.2Ca–3Zn alloy. Ceramics International, 2015, 41, 15272-15277.	2.3	24
50	Essential Magnesium Alloys Binary Phase Diagrams and Their Thermochemical Data. Journal of Materials, 2014, 2014, 1-33.	0.1	76
51	Experimental Investigation of the Phase Equilibria in the Al-Mn-Zn System at 400°C. Journal of Materials, 2014, 2014, 1-13.	0.1	6
52	Progress in Wettability Study of Reactive Systems. Journal of Metallurgy, 2014, 2014, 1-14.	1.1	8
53	Phase Equilibria of the Ce-Mg-Zn Ternary System at 300 °C. Metals, 2014, 4, 168-195.	1.0	7
54	Influence of Cooling Rate on Microsegregation Behavior of Magnesium Alloys. Journal of Materials, 2014, 2014, 1-18.	0.1	99

#	Article	IF	CITATIONS
55	Laser Peening Process and Its Impact on Materials Properties in Comparison with Shot Peening and Ultrasonic Impact Peening. Materials, 2014, 7, 7925-7974.	1.3	286
56	Effect of heat treatment on the microstructure and corrosion behaviour of Mg–Zn alloys. Materials and Corrosion - Werkstoffe Und Korrosion, 2014, 65, 999-1006.	0.8	32
57	Microstructure and bioâ€corrosion behavior of Mg–Zn and Mg–Zn–Ca alloys for biomedical applications. Materials and Corrosion - Werkstoffe Und Korrosion, 2014, 65, 1178-1187.	0.8	96
58	Tensile properties of laser additive manufactured Inconel 718 using filler wire. Journal of Materials Research, 2014, 29, 2006-2020.	1.2	36
59	On the atomic interdiffusion in Mg–{Ce, Nd, Zn} and Zn–{Ce, Nd} binary systems. Journal of Materials Research, 2014, 29, 1463-1479.	1.2	15
60	Effect of Casting Parameters on the Microstructural and Mechanical Behavior of Magnesium AZ31-B Alloy Strips Cast on a Single Belt Casting Simulator. Advances in Materials Science and Engineering, 2014, 2014, 1-9.	1.0	0
61	Global and Local Mechanical Properties of Autogenously Laser Welded Ti-6Al-4V. Metallurgical and Materials Transactions A: Physical Metallurgy and Materials Science, 2014, 45, 1258-1272.	1.1	20
62	Experimental and thermodynamic study of the Mg–Sn–In–Zn quaternary system. Journal of Alloys and Compounds, 2014, 588, 75-95.	2.8	17
63	Fabrication and corrosion behavior of Si/HA nano-composite coatings on biodegradable Mg–Zn–Mn–Ca alloy. Surface and Coatings Technology, 2014, 258, 1090-1099.	2.2	48
64	In-vitro degradation behavior of Mg alloy coated by fluorine doped hydroxyapatite and calcium deficient hydroxyapatite. Transactions of Nonferrous Metals Society of China, 2014, 24, 2516-2528.	1.7	39
65	Experimental investigation of the Mg–Mn–Nd isothermal section at 450°C. Journal of Alloys and Compounds, 2014, 608, 247-257.	2.8	2
66	Critical assessment and thermodynamic modeling of Mg–Ca–Zn system supported by key experiments. Calphad: Computer Coupling of Phase Diagrams and Thermochemistry, 2014, 46, 134-147.	0.7	20
67	Experimental Investigation of the Ce-Mg-Mn Isothermal Section at 723ÂK (450°C) via Diffusion Couples Technique. Metallurgical and Materials Transactions A: Physical Metallurgy and Materials Science, 2014, 45, 3144-3160.	1.1	3
68	Thermodynamic and Experimental Study of the Mg-Sn-Ag-In Quaternary System. Journal of Phase Equilibria and Diffusion, 2014, 35, 284-313.	0.5	22
69	In-vitro corrosion inhibition mechanism of fluorine-doped hydroxyapatite and brushite coated Mg–Ca alloys for biomedical applications. Ceramics International, 2014, 40, 7971-7982.	2.3	87
70	Synthesis and biodegradation evaluation of nano-Si and nano-Si/TiO2 coatings on biodegradable Mg–Ca alloy in simulated body fluid. Ceramics International, 2014, 40, 14009-14018.	2.3	32
71	Enhancement of amorphous phase formation in alumina–YSZ coatings deposited by suspension plasma spray process. Surface and Coatings Technology, 2013, 220, 191-198.	2.2	23
72	Experimental study of the Cu–Ni–Y system at 700 °C using diffusion couples and key alloys. Journal of Alloys and Compounds, 2013, 561, 161-173.	2.8	8

#	Article	IF	CITATIONS
73	Experimental investigation and first-principle calculations coupled with thermodynamic modeling of the Mn–Nd phase diagram. Calphad: Computer Coupling of Phase Diagrams and Thermochemistry, 2013, 42, 27-37.	0.7	5
74	Al–Mg–RE (RE=La, Ce, Pr, Nd, Sm) systems: Thermodynamic evaluations and optimizations coupled with key experiments and Miedema's model estimations. Journal of Chemical Thermodynamics, 2013, 58, 166-195.	1.0	45
75	Crystallization characteristics of the Mg-rich metallic glasses in the Ca–Mg–Zn system. Journal of Alloys and Compounds, 2013, 552, 88-97.	2.8	23
76	On the prediction of Gibbs free energy of mixing of binary liquid alloys. Journal of Chemical Thermodynamics, 2013, 57, 82-91.	1.0	19
77	Distortion and residual stress measurements of induction hardened AISI 4340 discs. Materials Chemistry and Physics, 2013, 142, 248-258.	2.0	21
78	Oxide films in laser additive manufactured Inconel 718. Acta Materialia, 2013, 61, 6562-6576.	3.8	93
79	Thermodynamic calculation of the Mg–Mn–Zn and Mg–Mn–Ce systems and re-optimization of their constitutive binaries. Calphad: Computer Coupling of Phase Diagrams and Thermochemistry, 2013, 41, 89-107.	0.7	20
80	Coherent nanoscale ternary precipitates in crystallized Ca4Mg72Zn24 metallic glass. Scripta Materialia, 2013, 68, 647-650.	2.6	8
81	Processing and Characterization of In Situ (TiC–TiB <sub>2</sub> ) <sub>p</sub> /AZ91D Magnesium Matrix Composites. Advanced Engineering Materials, 2013, 15, 708-717.	1.6	2
82	Phase equilibrium in Mg-Cu-Y. Scientific Reports, 2013, 3, 3033.	1.6	9
83	Synthesizing Nanostructured Ni <sub>75</sub> Mg <sub>16.66</sub> Y <sub>8.34</sub> (at%) Powder by Solid State Reaction and Mechanical Milling. Materials and Manufacturing Processes, 2012, 27, 1300-1305.	2.7	8
84	Use of filler wire for laser welding of Ti–6Al–4V. Canadian Metallurgical Quarterly, 2012, 51, 320-327.	0.4	13
85	Homogeneity range and crystal structure of the Ca2Mg5Zn13 compound. Journal of Alloys and Compounds, 2012, 523, 75-82.	2.8	12
86	Experimental investigation of the phase equilibria of the Al–Ca–Zn system at 623K. Journal of Alloys and Compounds, 2012, 539, 97-102.	2.8	2
87	Critical assessment and thermodynamic modeling of Mg–Zn, Mg–Sn, Sn–Zn and Mg–Sn–Zn systems. Calphad: Computer Coupling of Phase Diagrams and Thermochemistry, 2012, 36, 28-43.	0.7	112
88	Effect of Postweld Heat Treatment on Microstructure, Hardness, and Tensile Properties of Laser-Welded Ti-6Al-4V. Metallurgical and Materials Transactions A: Physical Metallurgy and Materials Science, 2012, 43, 4171-4184.	1.1	56
89	Thermal Cycling of Suspension Plasma Sprayed Aluminaâ€ <scp><scp>YSZ</scp></scp> Coatings Containing Amorphous Phases. Journal of the American Ceramic Society, 2012, 95, 2614-2621.	1.9	13
90	Understanding the reaction mechanism of in-situ synthesized (TiC–TiB2)/AZ91 magnesium matrix composites. Materials Chemistry and Physics, 2012, 135, 193-205.	2.0	33

#	Article	IF	CITATIONS
91	Experimental study of the Ca–Mg–Zn system using diffusion couples and key alloys. Science and Technology of Advanced Materials, 2011, 12, 025003.	2.8	30
92	Crashworthiness improvement of a pickup truck's chassis frame using the Pareto-Front and genetic algorithm. International Journal of Heavy Vehicle Systems, 2011, 18, 83.	0.1	3
93	Structural considerations in plasma spraying of the alumina–zirconia composite. Surface and Coatings Technology, 2011, 205, 5437-5443.	2.2	14
94	Amorphous and crystalline phase formation during suspension plasma spraying of the alumina–zirconia composite. Journal of the European Ceramic Society, 2011, 31, 2903-2913.	2.8	61
95	Highâ€Temperature Performance of Alumina–Zirconia Composite Coatings Containing Amorphous Phases. Advanced Functional Materials, 2011, 21, 4143-4151.	7.8	48
96	The effect of cooling rate on thermophysical properties of magnesium alloys. Journal of Materials Research, 2011, 26, 974-982.	1.2	14
97	Novel fabrication process of AlN ceramic matrix composites at low temperatures. Science and Engineering of Composite Materials, 2011, 18, .	0.6	1
98	Phase Formation and Transformation in Alumina/YSZ Nanocomposite Coating Deposited by Suspension Plasma Spray Process. Journal of Thermal Spray Technology, 2010, 19, 787-795.	1.6	38
99	The 400°C isothermal section of the Mg–Al–Ca system. Intermetallics, 2010, 18, 1498-1506.	1.8	21
100	Determination of the solubility range and crystal structure of the Mg-rich ternary compound in the Ca–Mg–Zn system. Intermetallics, 2010, 18, 2404-2411.	1.8	37
101	Phase equilibria of the constituent ternaries of the Mg-Al-Ca-Sr system. Jom, 2009, 61, 68-74.	0.9	11
102	A critical thermodynamic assessment of the Mg–Ni, Ni–Y binary and Mg–Ni–Y ternary systems. Calphad: Computer Coupling of Phase Diagrams and Thermochemistry, 2009, 33, 478-486.	0.7	53
103	A thermodynamic description of the Al–Ca–Zn ternary system. Calphad: Computer Coupling of Phase Diagrams and Thermochemistry, 2009, 33, 584-598.	0.7	17
104	Critical assessment and thermodynamic modeling of the binary Mg–Zn, Ca–Zn and ternary Mg–Ca–Zn systems. Intermetallics, 2009, 17, 847-864.	1.8	88
105	Thermodynamic Description of the Mg-Mn, Al-Mn and Mg-Al-Mn Systems Using the Modified Quasichemical Model for the Liquid Phases. Materials Transactions, 2009, 50, 1113-1122.	0.4	36
106	The equilibrium phase diagram of the magnesium–copper–yttrium system. Journal of Chemical Thermodynamics, 2008, 40, 1064-1076.	1.0	33
107	Effective Parameters in Axial Injection Suspension Plasma Spray Process of Alumina-Zirconia Ceramics. Journal of Thermal Spray Technology, 2008, 17, 685-691.	1.6	57
108	Experimental Demonstration of Entrance/Exit Effects on the Permeability Measurements of Porous Materials. Advanced Engineering Materials, 2008, 10, 889-894.	1.6	44

#	Article	IF	CITATIONS
109	Thermodynamic assessment of the phase equilibria in the Al–Ca–Sr system using the modified quasichemical model. Journal of Chemical Thermodynamics, 2008, 40, 724-734.	1.0	11
110	Nd:YAG laser welding of aerospace grade ZE41A magnesium alloy: Modeling and experimental investigations. Materials Chemistry and Physics, 2008, 109, 61-76.	2.0	46
111	Thermodynamic modelling of the Mg–Ca, Mg–Sr, Ca–Sr and Mg–Ca–Sr systems using the modified quasichemical model. Calphad: Computer Coupling of Phase Diagrams and Thermochemistry, 2008, 32, 240-251.	0.7	62
112	An Efficient Crashworthiness Design Optimization Approach for Frontal Automobile Structures. , 2008, , .		0
113	Reliability of Laser Welding Process for ZE41A-T5 Magnesium Alloy Sand Castings. Materials Transactions, 2008, 49, 774-781.	0.4	6
114	New Phases in the Mg-Al-Sr System. Materials Science Forum, 2007, 539-543, 1620-1625.	0.3	2
115	Experimental investigation of the MgAlCa system. Journal of Alloys and Compounds, 2007, 436, 131-141.	2.8	50
116	Thermodynamic assessment of the Mg–Zn–Sr system. Intermetallics, 2007, 15, 93-97.	1.8	16
117	Experimental study and thermodynamic calculation of Al–Mg–Sr phase equilibria. Intermetallics, 2007, 15, 506-519.	1.8	40
118	Microstructural characterization of Mg–Al–Sr alloys. Science and Technology of Advanced Materials, 2007, 8, 237-248.	2.8	21
119	Transient liquid phase bonding of Inconel 718 and Inconel 625 with BNi-2: Modeling and experimental investigations. Materials Science & Engineering A: Structural Materials: Properties, Microstructure and Processing, 2007, 447, 125-133.	2.6	136
120	Effect of alloying elements on the isothermal solidification during TLP bonding of SS 410 and SS 321 using a BNi-2 interlayer. Materials Chemistry and Physics, 2007, 106, 109-119.	2.0	44
121	The effect of microstructure on the permeability of metallic foams. Journal of Materials Science, 2007, 42, 4372-4383.	1.7	58
122	A computational thermodynamic model of the Mg–Al–Ge system. Journal of Alloys and Compounds, 2006, 425, 129-139.	2.8	23
123	High temperature neutron diffraction study of the Al2O3–Y2O3 system. Journal of the European Ceramic Society, 2006, 26, 3515-3524.	2.8	107
124	Thermodynamic modeling of the Ca–Ni system. Science and Technology of Advanced Materials, 2006, 7, 119-126.	2.8	4
125	Computational thermodynamic model for the Mgâ^'Alâ^'Y system. Journal of Phase Equilibria and Diffusion, 2006, 27, 231-244.	0.5	25
126	Mathematical Modeling and Experimental Investigations of Isothermal Solidification during Transient Liquid Phase Bonding of Nickel Superalloys. Advanced Materials Research, 2006, 15-17, 882-887.	0.3	1

#	Article	IF	CITATIONS
127	THERMODYNAMIC MODELLING OF THE Mg-Al-Ca SYSTEM. Canadian Metallurgical Quarterly, 2005, 44, 523-536.	0.4	16
128	Understanding AlN sintering through computational thermodynamics combined with experimental investigation. Journal of Materials Processing Technology, 2005, 161, 415-422.	3.1	38
129	Experimental study of the ternary magnesium–aluminium–strontium system. Journal of Alloys and Compounds, 2005, 402, 170-185.	2.8	30
130	Thermodynamic modeling of the Mg–Al–Sb system. Calphad: Computer Coupling of Phase Diagrams and Thermochemistry, 2005, 29, 24-36.	0.7	41
131	The phase equilibria in the Mg–Ni–Ca system. Calphad: Computer Coupling of Phase Diagrams and Thermochemistry, 2005, 29, 289-302.	0.7	29
132	Highâ€Temperature Neutron Diffraction of the AlN–Al <sub>2</sub> O <sub>3</sub> –Y <sub>2</sub> O <sub>3</sub> System. Journal of the American Ceramic Society, 2003, 86, 717-26.	1.9	13
133	The equilibria in the AlN-Al 2 O 3 -Y 2 O 3 system - thermodynamics and neutron diffraction. Applied Physics A: Materials Science and Processing, 2002, 74, s1188-s1191.	1.1	1
134	Morphological and Crystallographic Characterizations of the Ca-Mg-Zn Intermetallics Appearing in Ternary Diffusion Couples. Advanced Materials Research, 0, 409, 387-392.	0.3	4
135	Ternary Intermetallic Compounds across the Mg-NiY Line at 673 K. Materials Science Forum, 0, 706-709, 1134-1139.	0.3	3
136	A Differential Scanning Calorimetric Study of the Mg-Cu-Y System. Materials Science Forum, 0, 706-709, 1215-1220.	0.3	1
137	Conversion of Electric Arc Furnace Dust into Ceramics Using Thermodynamic Calculations and Experimental Work Key Engineering Materials 0, 765, 73-78	0.4	2